INTERNATIONAL JOURNAL FOR NUMERICAL AND ANALYTICAL METHODS IN GEOMECHANICS
Int. J. Numer. Anal. Meth. Geomech. 2008; **32**:415–436
Published online 13 June 2007 in Wiley InterScience (www.interscience.wiley.com). DOI: 10.1002/nag.631

A stepwise damping-solvent extraction method for large-scale dynamic soil–structure interaction analysis in time domain

J. B. Li[1], J. Yang[2,*,†] and G. Lin[1]

[1]*School of Civil and Hydraulic Engineering, Dalian University of Technology, Dalian, China*
[2]*Department of Civil Engineering, The University of Hong Kong, Hong Kong, China*

SUMMARY

Time-domain analysis of dynamic soil–structure interaction based on the substructure method plays an increasing role in practical applications as compared with the frequency-domain analysis. Efficient and accurate modelling of the unbounded soil or rock medium has been a key issue in such an analysis. This paper presents a subregional stepwise damping-solvent extraction formulation for solving large-scale dynamic soil–structure problems in the time domain. Accuracy and efficiency of the formulation are evaluated in detail for a classical problem involving a rigid strip foundation embedded in a half-space. A practical large-scale soil–structure interaction problem, which represents a high concrete gravity dam subjected to seismic load, is then analysed using the proposed method. Various responses of the dam, including time histories of the crest displacement and acceleration and contours of the peak principal stresses within the dam body, are presented. Comparisons are also made between these results with those obtained using other models for the unbounded medium. Copyright © 2007 John Wiley & Sons, Ltd.

Received 22 August 2006; Revised 15 April 2007; Accepted 15 April 2007

KEY WORDS: soil–structure interaction; time-domain analysis; wave propagation; damping effect

1. INTRODUCTION

A typical dynamic soil–structure interaction problem involves a structure supported by an unbounded soil medium and subjected to a time-varying earthquake load. Efficient yet accurate modelling of the unbounded soil medium has been of long-standing interest in research on dynamic soil–structure interaction. There are generally two major methods for analysis of the dynamic system [1]: the direct method and the substructure method. Accumulating experience

*Correspondence to: J. Yang, Department of Civil Engineering, The University of Hong Kong, Hong Kong, China.
†E-mail: junyang@hku.hk

Contract/grant sponsor: Natural Science Foundation of China; contract/grant number: 90510018
Contract/grant sponsor: Research Grants Council of Hong Kong; contract/grant number: HKU7191/05E

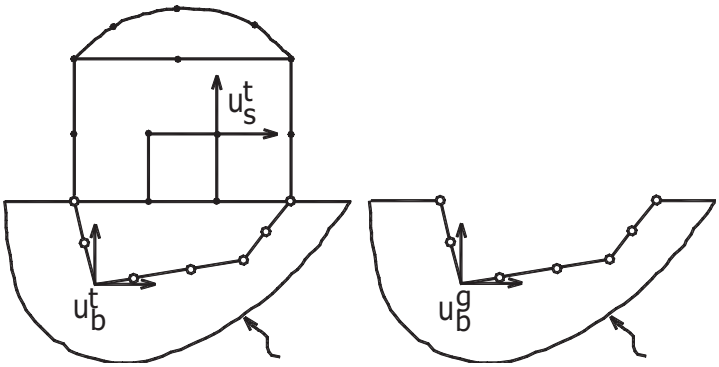

Figure 1. Dynamic soil–structure interaction system.

indicates that while the direct method is a conceptually easier way to model the entire soil–structure system in a single step, the substructure method is computationally more efficient. In the substructure method, the soil–structure system is divided into two parts: one part is the generalized structure including a portion of adjacent soil with an irregular boundary, which can behave nonlinearly; the other part is the semi-infinite, unbounded linear soil medium (see Figure 1). The generalized soil–structure interface separates the two parts.

The substructure method consists of three major steps. First, the seismic free-field input motion on the soil–structure interface is determined. Second, the reaction of the unbounded soil on the interface is determined in the form of a displacement–force relationship. Third, the bounded soil–structure system under the interaction force is analysed.

Analysis of the soil involves the solution of a wave propagation problem with the radiation condition imposed as a boundary condition at infinity. It is the numerical implementation of the radiation condition that poses a challenge in such an analysis. There are traditionally two ways for implementation of the radiation condition: one way is to enforce the condition rigorously at the soil–structure interface by using the boundary element technique [2, 3], and the other way is to impose a wave absorbing boundary condition on the outer boundary of a bounded domain [4–7]. Recently, a novel method for the analysis of the unbounded soil medium, known as the damping-solvent extraction (DSE) method, was suggested by Wolf and Song [8]. The method, developed based on the physical notion that waves propagating in a damped medium decay, seeks to simulate approximately the radiation condition by using artificial material damping to attenuate both outgoing and reflected waves, and then 'extracting' the artificial damping in order to remove its undesirable effects.

The DSE method has been evaluated in detail in the frequency domain for three classical problems [8, 9], i.e. the problem of out-of-plane motion of a semi-infinite layer of constant depth, the problem of in-plane motion of a semi-infinite wedge, and the problem of a strip foundation with rectangular cross-section embedded in a half-plane. Feasibility of the DSE method in the time-domain analysis was briefly discussed for the third problem [8] where no real structures were involved. Time-domain 'implementation of the method for analysing practical, large-scale dynamic interaction problems is a challenging task; this is due partly to the fact that the time-domain formulation usually involves convolution integrals causing the solution to be very complicated [1, 10].

DOI: 10.1002/nag

The objective of this paper is to present an efficient and accurate subregional stepwise DSE scheme for the dynamic analysis of large-scale soil–structure interaction problems in the time domain. This paper is organized as follows. First, the principle of the DSE method is briefly reviewed and its time-domain implementation is outlined. This is followed by a complete description of the subregional stepwise DSE formulation in the time domain. Finally, the performance of the proposed formulation is assessed in detail and a large-scale dynamic soil–structure interaction problem is analysed.

2. PRINCIPLE OF DAMPING-SOLVENT EXTRACTION METHOD

The DSE method is conceptually simple and involves three major steps. In the first step, a finite region adjacent to the soil–structure interface is selected and discretized using the finite element technique (see Figure 2). Artificial material damping that is not present in the actual medium is added as a solvent to attenuate outgoing and reflected waves. The outer boundary of the finite region is usually defined as an absorbing boundary to decay the waves further. The second step involves computation of the dynamic stiffness of the bounded domain at the soil–structure interface. In the third step, the influence of artificial damping on the dynamic stiffness derived in the second step is extracted, resulting in the dynamic stiffness for unbounded domain.

In the frequency domain, the dynamic stiffness matrix of the unbounded domain $[S^{\infty}(\omega)]$ can be derived in relation to the dynamic stiffness of the artificially damped bounded domain $[S_{\xi}(\omega)]$ as [8]

$$[S^{\infty}(\omega)] = \frac{G}{G^*}\left([S_{\xi}(\omega)] + [S_{\xi}(\omega)]_{,\omega}\frac{(a_0 - a_0^*)}{a_{0,\omega}^*}\right) \tag{1}$$

where G and G^* are shear moduli of the natural medium and the artificially damped medium, respectively; a_0 and a_0^* are dimensionless frequencies for the natural medium and the artificially damped medium, respectively; a comma represents the derivative with respect to the corresponding variable. G^* and a_0^* are defined as follows: $G^* = G(1 + 2\mathrm{i}\xi)$ and $a_0^* = \omega r_0/(c_s\sqrt{1 + 2\mathrm{i}\xi})$, where ω is the excitation frequency, r_0 is the characteristic length, c_s is the shear wave velocity of the undamped medium, and ξ is the linear material hysteretic damping.

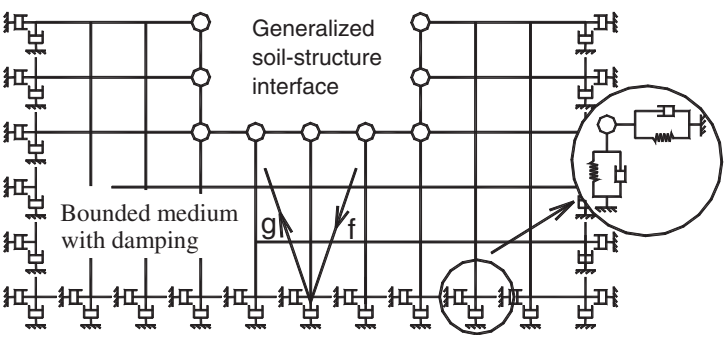

Figure 2. FE model of finite region of unbounded medium.

DOI: 10.1002/nag

For a time-domain analysis, the interior material hysteretic damping is not considered suitable; rather, the exterior mass-proportional dashpots, equivalently defined as a damping matrix $2\zeta[M]$ and an additional stiffness matrix $\zeta^2[M]$, can be chosen for the bounded medium to provide the artificial damping. The nodal damping coefficient ζ has the dimension of c_s/r_0. The dynamic stiffness matrix of the unbounded domain $[S^\infty(\omega)]$ can be formulated in a similar form to that for the frequency-domain implementation [8]

$$[S^\infty(\omega)] = [S_\zeta(\omega)] + [S_\zeta(\omega)]_{,\omega} \frac{(a_0 - a_0^*)}{a_{0,\omega}^*} \tag{2}$$

with $G^* = G$ and the dimensionless frequency, a_0^* defined as

$$a_0^* = \frac{(\omega - \mathrm{i}\zeta) r_0}{c_s} \tag{3}$$

Substituting Equation (3) into Equation (2) gives

$$[S^\infty(\omega)] = [S_\zeta(\omega)] + \mathrm{i}\zeta [S_\zeta(\omega)]_{,\omega} \tag{4}$$

Applying the inverse Fourier transformation to Equation (4) yields the impulse displacement response as

$$[S^\infty(t)] = (1 + \zeta t)[S_\zeta(t)] \tag{5}$$

The interaction force of the undamped unbounded medium $\{R^\infty(t)\}$ can then be determined by

$$\{R^\infty(t)\} = \int_0^t [S^\infty(t - \tau)]\{u(\tau)\}\,\mathrm{d}\tau \tag{6}$$

Substituting Equation (5) into Equation (6) results in

$$\{R^\infty(t)\} = (1 + \zeta t)\{R_\zeta(t)\} - \zeta\{R_{\zeta r}(t)\} \tag{7}$$

It becomes apparent from Equation (7) that the interaction force consists of two components: one is the interaction force of the damped bounded medium for the original loading $\{u(t)\}$ at the soil–structure interface

$$\{R_\zeta(t)\} = \int_0^t [S_\zeta(t - \tau)]\{u(\tau)\}\,\mathrm{d}\tau \tag{8}$$

and the other component is the interaction force of the damped bounded medium for the loading $\{u_r(t)\} = t\{u(t)\}$ at the soil–structure interface:

$$\{R_{\zeta r}(t)\} = \int_0^t [S_\zeta(t - \tau)]\{u_r(\tau)\}\,\mathrm{d}\tau \tag{9}$$

3. SUBREGIONAL STEPWISE IMPLEMENTATION IN TIME DOMAIN

3.1. Computation of dynamic interaction force

Direct computation of the interaction force based on Equations (7)–(9) requires significant computational effort because of the convolution integrals involved. Rather than using the direct procedure,

DOI: 10.1002/nag

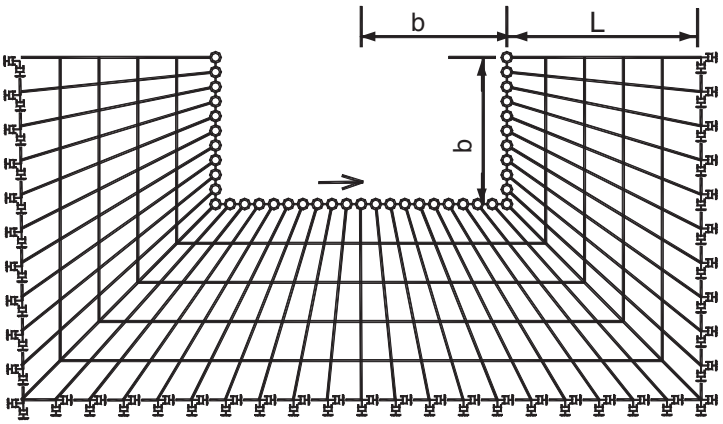

Figure 3. FE discretization of bounded medium for time-domain analysis.

the interaction forces $\{R_\zeta(t)\}$ and $\{R_{\zeta r}(t)\}$ can be calculated using the following discrete equation of motion for the artificially damped bounded region:

$$[\overline{M}]\{\ddot{u}\} + [\overline{C}]\{\dot{u}\} + [\overline{K}]\{u\} = \{R\} \tag{10}$$

where $[\overline{M}] = [M]$, $[\overline{C}] = 2\zeta[M]$, $[\overline{K}] = [K] + \zeta^2[M]$ are the mass, damping and stiffness matrices, respectively, and $\{R\}$ is the load vector.

Though the convolution integrals can be avoided by using Equation (10), it should be noted, however, that both Equation (7) and the relationship $\{u_r(t)\} = t\{u(t)\}$ contain the absolute time variable t. The inclusion of the time variable t in the formulation may cause numerical difficulties and inaccuracies in the computation. For example, the structural current response may be affected by the selection of the starting point of the absolute time variable t and numerical errors may be magnified with increasing time steps. To deal with this problem, effort is made to develop an explicit formulation that eliminates the absolute time variable.

In doing that, Equation (10) is rewritten in the form of partition matrices by introducing Equation (8)

$$\begin{Bmatrix} 0 \\ R_{\zeta b} \end{Bmatrix} = \begin{bmatrix} \overline{M}_{mm} & 0 \\ 0 & \overline{M}_{bb} \end{bmatrix} \begin{Bmatrix} \ddot{u}_m \\ \ddot{u}_b \end{Bmatrix} + \begin{bmatrix} \overline{C}_{mm} & 0 \\ 0 & \overline{C}_{bb} \end{bmatrix} \begin{Bmatrix} \dot{u}_m \\ \dot{u}_b \end{Bmatrix} + \begin{bmatrix} \overline{K}_{mm} & \overline{K}_{mb} \\ \overline{K}_{bm} & \overline{K}_{bb} \end{bmatrix} \begin{Bmatrix} u_m \\ u_b \end{Bmatrix} \tag{11}$$

where the subscripts b and m denote the nodes on the generalized soil–structure interface and the nodes inside the bounded medium, respectively.

The above equation can be further rewritten as two sub-equations:

$$-[\overline{K}_{mb}]\{u_b\} = [\overline{M}_{mm}]\{\ddot{u}_m\} + [\overline{C}_{mm}]\{\dot{u}_m\} + [\overline{K}_{mm}]\{u_m\} \tag{12}$$

$$\{R_{\zeta b}\} = [\overline{M}_{bb}]\{\ddot{u}_b\} + [\overline{C}_{bb}]\{\dot{u}_b\} + [\overline{K}_{bb}]\{u_b\} + [\overline{K}_{bm}]\{u_m\} \tag{13}$$

DOI: 10.1002/nag

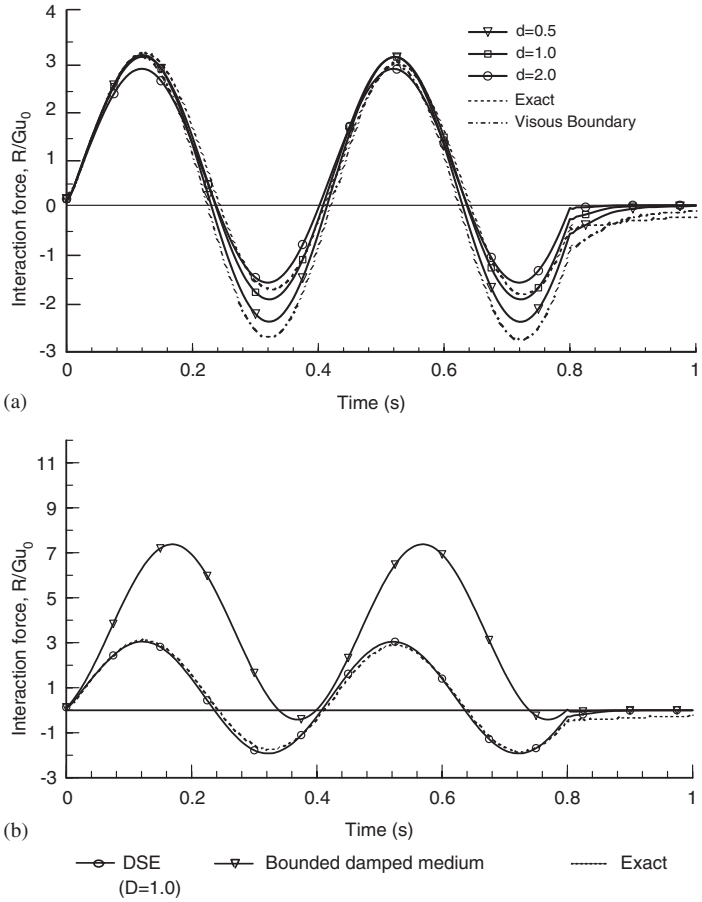

Figure 4. Computed time history of interaction force: (a) effect of artificial damping and (b) effect of damping extraction.

Similarly, introducing Equation (9) into Equation (10) leads to

$$\begin{Bmatrix} 0 \\ R_{r\zeta b} \end{Bmatrix} = \begin{bmatrix} \overline{K}_{mm} & \overline{K}_{mb} \\ \overline{K}_{bm} & \overline{K}_{bb} \end{bmatrix} \begin{Bmatrix} u_{rm} \\ u_{rb} \end{Bmatrix} + \begin{bmatrix} \overline{C}_{mm} & 0 \\ 0 & \overline{C}_{bb} \end{bmatrix} \begin{Bmatrix} \dot{u}_m \\ \dot{u}_{rb} \end{Bmatrix} + \begin{bmatrix} \overline{M}_{mm} & 0 \\ 0 & \overline{M}_{bb} \end{bmatrix} \begin{Bmatrix} \ddot{u}_{rm} \\ \ddot{u}_{rb} \end{Bmatrix} \tag{14}$$

where $\{u_{rb}\} = t\{u_b\}$.

The first- and second-order derivatives of $\{u_{rb}\}$ with respect to time can be readily given by

$$\{\dot{u}_{rb}\} = t\{\dot{u}_b\} + \{u_b\} \tag{15}$$

$$\{\ddot{u}_{rb}\} = 2\{\dot{u}_b\} + t\{\ddot{u}_b\} \tag{16}$$

To eliminate the variable t in the formulation, an assumption is made herein for the nodal displacements inside the bounded medium, $\{u_{rm}\}$, such that

$$\{u_{rm}\} = t\{u_m\} - \{v_m\} \tag{17}$$

DOI: 10.1002/nag

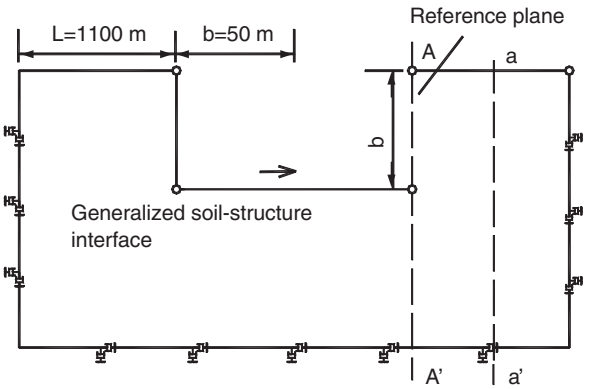

Figure 5. A finite region of unbounded medium used in Example 3.

Accordingly, the time derivatives of $\{u_{rm}\}$ can be given as

$$\{\dot{u}_{rm}\} = t\{\dot{u}_m\} + \{u_m\} - \{\dot{v}_m\} \tag{18}$$

$$\{\ddot{u}_{rm}\} = 2\{\dot{u}_m\} + t\{\ddot{u}_m\} - \{\ddot{v}_m\} \tag{19}$$

Substituting Equations (15)–(19) into Equation (14) leads to

$$[\overline{M}_{mm}]\{\ddot{v}_m\} + [\overline{C}_{mm}]\{\dot{v}_m\} + [\overline{K}_{mm}]\{v_m\} = 2[\overline{M}_{mm}]\{\dot{u}_m\} + [\overline{C}_{mm}]\{u_m\} \tag{20}$$

$$\{R_{r\zeta b}\} = t\{R_{\zeta b}\} + 2[\overline{M}_{bb}]\{\dot{u}_b\} + [\overline{C}_{bb}]\{u_b\} - [\overline{K}_{bm}]\{v_m\} \tag{21}$$

Finally, the interaction force in the time domain can be determined as

$$\begin{aligned}\{R^{\infty}(t)\} = {} & [\overline{M}_{bb}]\{\ddot{u}_b\} + ([\overline{C}_{bb}] - 2\zeta[\overline{M}_{bb}])\{\dot{u}_b\} \\ & + ([\overline{K}_{bb}] - \zeta[\overline{C}_{bb}])\{u_b\} + [\overline{K}_{bm}]\{u_m\} + \zeta[\overline{K}_{bm}]\{v_m\}\end{aligned} \tag{22}$$

Note that Equation (22) eliminates the absolute time variable t and the interaction force $\{R^{\infty}(t)\}$ can be conveniently computed by employing a step-by-step integration algorithm. Also, note that $\{u_m\}$ and $\{v_m\}$ can be computed based on Equations (12) and (20) while $\{u_b\}$ can be solved by combining Equation (22) with the equation of motion of the generalized structure.

3.2. Computation of dynamic response of structure

Now, consider the generalized structure that may include an adjacent, irregular soil region and may behave nonlinearly. The discrete equation of motion of the system can be expressed as

$$\begin{bmatrix}[M_{ss}] & [M_{sb}] \\ [M_{bs}] & [M_{bb}]\end{bmatrix}\begin{Bmatrix}\{\ddot{u}_s^{\mathrm{al}}(t)\} \\ \{\ddot{u}_b^{\mathrm{al}}(t)\}\end{Bmatrix} + \begin{Bmatrix}\{P_s(t)\} \\ \{P_b(t)\}\end{Bmatrix} = \begin{Bmatrix}\{0\} \\ \{-R_b(t)\}\end{Bmatrix} \tag{23}$$

where the superscript al denotes the total motion, $\{P(t)\}$ is the vector of the nonlinear internal forces of the system at time t, $\{R_b(t)\}$ is the vector of the interaction forces and is a function of

DOI: 10.1002/nag

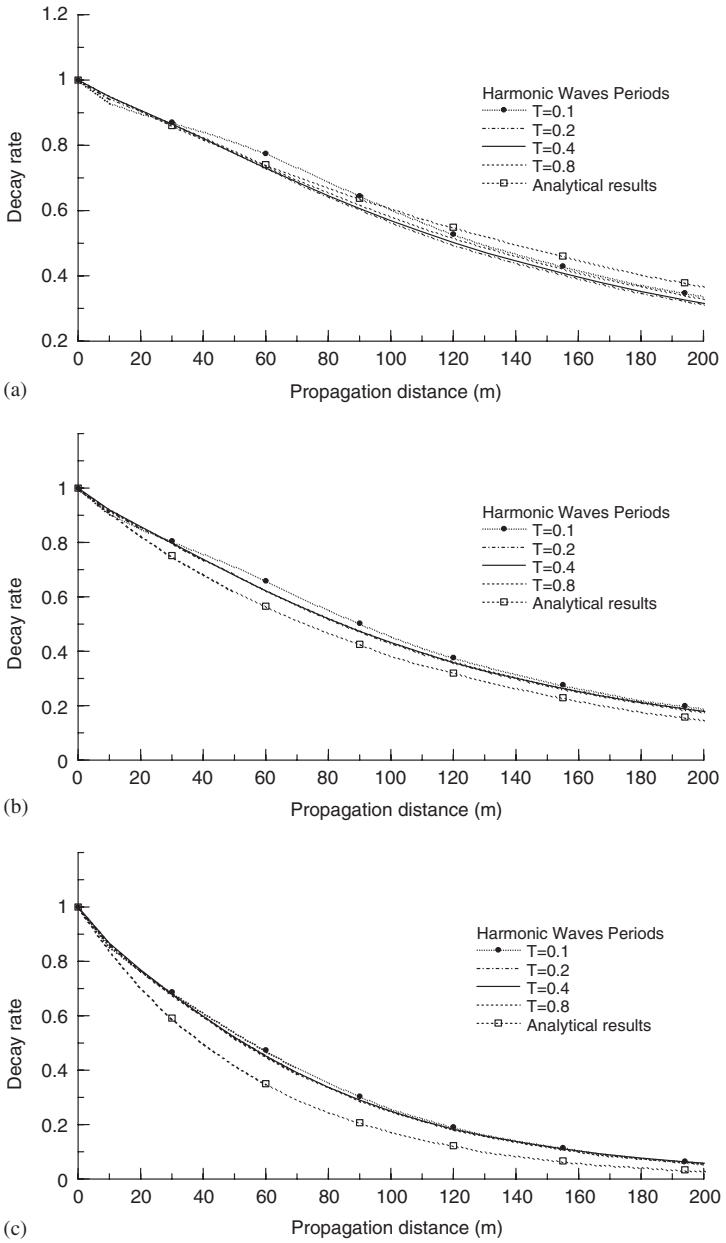

Figure 6. Amplitude decay of outgoing waves: (a) $d = 0.25$; (b) $d = 0.5$; and (c) $d = 1.0$.

the motion relative to the ground, i.e.

$$\{R_b(t)\} = \int [S_{bb}^{\infty}(t-\tau)](\{u_b^{\mathrm{al}}(\tau)\} - \{u_b^{\mathrm{g}}(\tau)\})\,\mathrm{d}\tau \tag{24}$$

DOI: 10.1002/nag

Table I. Propagation distance for a decay rate of 50%.

Artificial damping factor, d	Propagation distance, L_{50}, (m)	Propagation distance normalized with wavelength			
		$T=0.1$ s	$T=0.2$ s	$T=0.4$ s	$T=0.8$ s
0.25	~120	1.2	0.6	0.3	0.15
0.5	~80	0.8	0.4	0.2	0.1
1.0	~40	0.4	0.2	0.1	0.05

Equation (23) can be reformulated by introducing Equation (24) as

$$\begin{bmatrix} [M_{ss}] & [M_{sb}] \\ [M_{bs}] & [M_{bb}] \end{bmatrix} \begin{Bmatrix} \ddot{u}_s^{\mathrm{al}}(t) \\ \ddot{u}_b^{\mathrm{al}}(t) \end{Bmatrix} + \begin{Bmatrix} P_s(t) \\ P_b(t) \end{Bmatrix} + \begin{Bmatrix} 0 \\ \displaystyle\int_0^t [S_{bb}^{\infty}(t-\tau)]\{u_b^{\mathrm{al}}(\tau)\}\,\mathrm{d}\tau \end{Bmatrix} = \begin{Bmatrix} 0 \\ \displaystyle\int_0^t [S_{bb}^{\infty}(t-\tau)]\{u_b^{\mathrm{g}}(\tau)\}\,\mathrm{d}\tau \end{Bmatrix} \tag{25}$$

The above equation describes a general procedure that can be used to compute various wave patterns consisting of inclined body waves and surface waves. In the case where the excavation is not involved (refer to Figure 1), the scattered motion $\{u_b^{\mathrm{g}}(t)\}$ can be replaced by the free-field ground motion $\{u_b^{\mathrm{f}}(t)\}$.

By introducing Equation (22) into Equation (23) or (25), the following equation of motion for the generalized structure system is obtained:

$$\begin{bmatrix} [M_{ss}^{\mathrm{s}}] & 0 \\ 0 & [M_{bb}^{*}] \end{bmatrix} \begin{Bmatrix} \ddot{u}_s^{\mathrm{al}} \\ \ddot{u}_b^{\mathrm{al}} \end{Bmatrix} + \begin{bmatrix} [C_{ss}^{\mathrm{s}}] & [C_{sb}^{\mathrm{s}}] \\ [C_{bs}^{\mathrm{s}}] & [C_{bb}^{*}] \end{bmatrix} \begin{Bmatrix} \dot{u}_b^{\mathrm{al}} \\ \dot{u}_b^{\mathrm{al}} \end{Bmatrix} + \begin{bmatrix} K_{ss}^{\mathrm{s}} & K_{sb}^{\mathrm{s}} \\ K_{bs}^{\mathrm{s}} & K_{bb}^{*} \end{bmatrix} \begin{Bmatrix} u_s^{\mathrm{al}} \\ u_b^{\mathrm{al}} \end{Bmatrix} = \begin{Bmatrix} 0 \\ [\overline{M}_{bb}]\{\ddot{u}_b^{\mathrm{g}}\} \end{Bmatrix} + \begin{Bmatrix} 0 \\ [\overline{C}_{bb}] - 2\zeta[\overline{M}_{bb}]\{\dot{u}_b^{\mathrm{g}}\} \end{Bmatrix} + \begin{Bmatrix} 0 \\ ([\overline{K}_{bb}] - \zeta[\overline{C}_{bb}])\{u_b^{\mathrm{g}}\} \end{Bmatrix} + \begin{Bmatrix} 0 \\ [\overline{K}_{bm}]\{u_m\} + \zeta[\overline{K}_{bm}]\{v_m\} \end{Bmatrix} \tag{26}$$

where

$$[M_{bb}^{*}] = [M_{bb}^{\mathrm{s}}] + [\overline{M}_{bb}] \tag{27}$$

$$[C_{bb}^{*}] = [C_{bb}^{\mathrm{s}}] + ([\overline{C}_{bb}] - 2\zeta[\overline{M}_{bb}]) \tag{28}$$

$$[K_{bb}^{*}] = [K_{bb}^{\mathrm{s}}] + ([\overline{K}_{bb}] - \zeta[\overline{C}_{bb}]) \tag{29}$$

As explained earlier, under the loading $\{u_b\} = \{u_b^{\mathrm{al}}\} - \{u_b^{\mathrm{g}}\}$ at the interface, $\{u_m\}$ and $\{v_m\}$ can be determined from Equations (12) and (20) using some integration scheme. In this study, the so-called predictor–corrector integration algorithm [11, 12] is adopted. This algorithm avoids the computation of the inverse of stiffness matrix and hence is particularly suitable for large-scale

DOI: 10.1002/nag

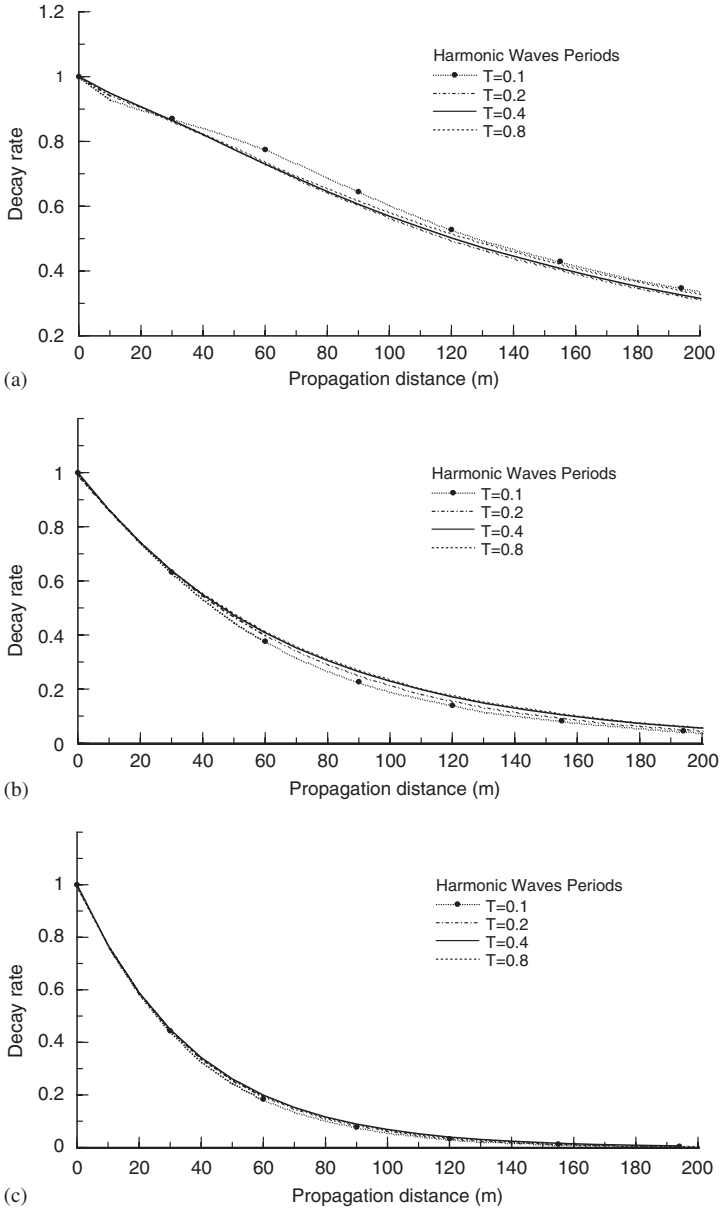

Figure 7. Kinetic energy decay of outgoing waves: (a) $d = 0.25$; (b) $d = 0.5$; and (c) $d = 1.0$.

dynamic problems. Numerical experiments have shown that convergence of the algorithm can be guaranteed under the condition of small time intervals. Thus, the response of the dynamic system can be solved step by step from Equation (26) for the prescribed seismic excitations $\{u_b^g\}$, $\{\dot{u}_b^g\}$ and $\{\ddot{u}_b^g\}$.

DOI: 10.1002/nag

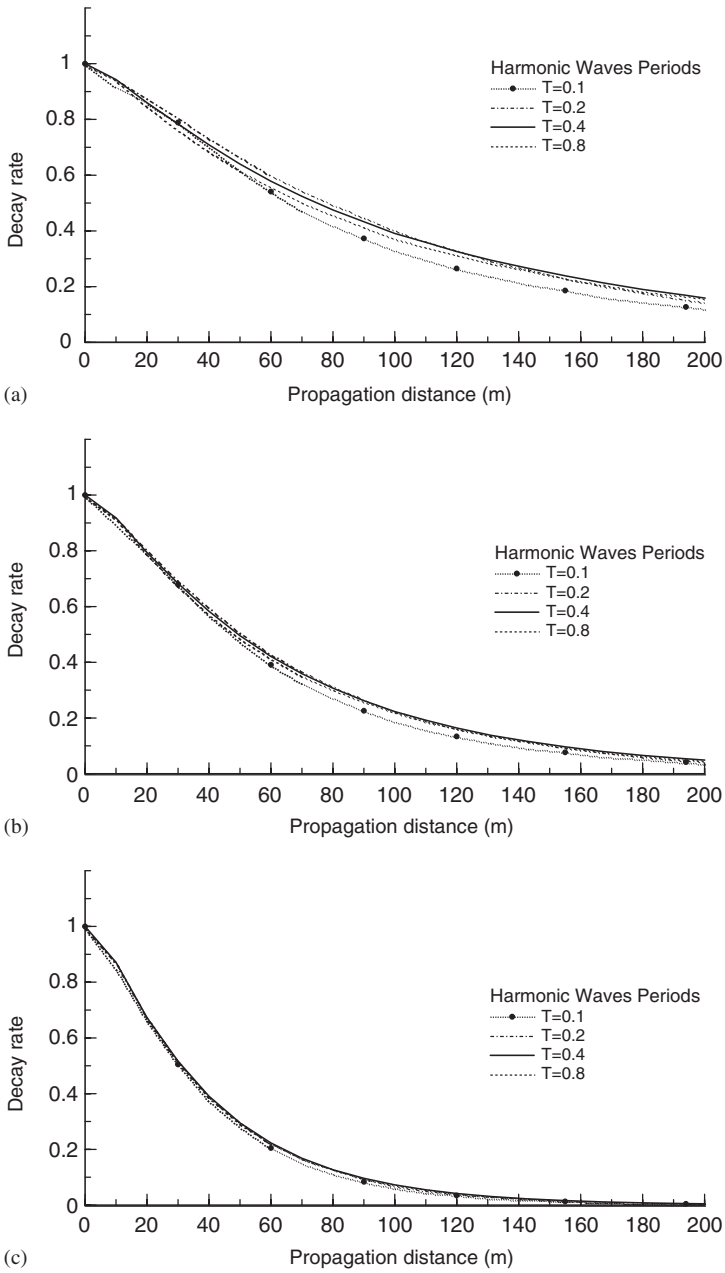

Figure 8. Potential energy decay of outgoing waves: (a) $d = 0.25$; (b) $d = 0.5$; and (c) $d = 1.0$.

It should be mentioned that in some cases only the earthquake ground acceleration $\{\ddot{u}_b^g\}$ is available for the analysis while the displacement and velocity excitations have to be obtained by integrating the acceleration. The direct integration of acceleration may cause unrealistic drifts

DOI: 10.1002/nag

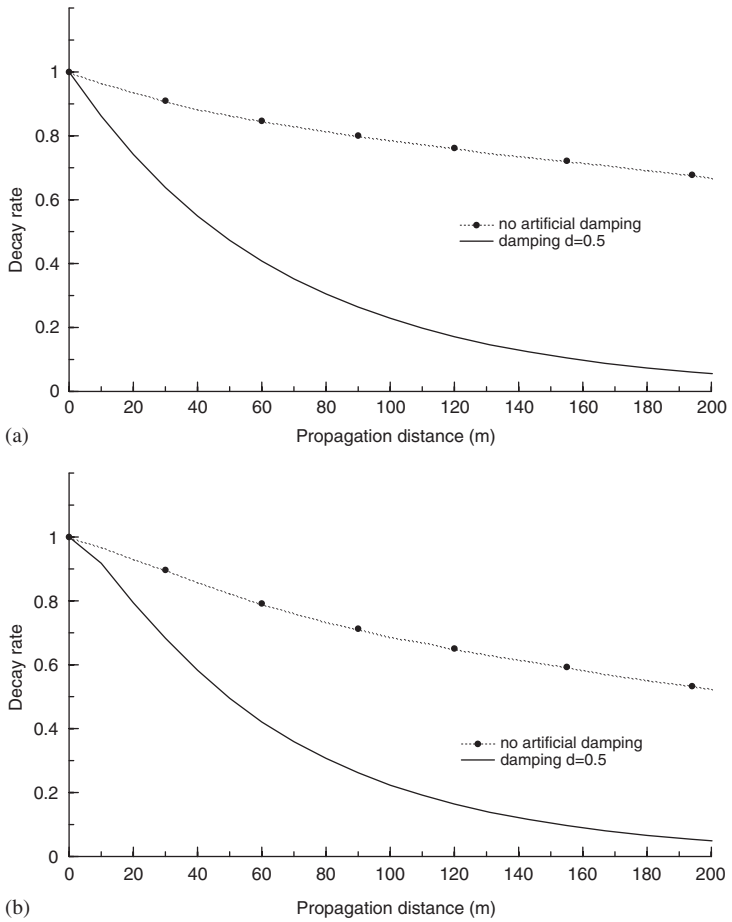

Figure 9. Decay of (a) kinetic and (b) potential energy due to artificial damping ($T = 0.4$ s).

in displacement and velocity [13–15]. Use of the drifted displacement and velocity as input motions may have a significant effect on the soil–structure interaction analysis. A simple approach suggested by Yang *et al*. [16], which involves the least-square curve fitting technique, can be used to directly process the acceleration time series to derive reasonable displacement and velocity excitations.

4. NUMERICAL EXAMPLES

A subregional stepwise DSE scheme for time-domain analysis of dynamic soil–structure interaction problems has been described. In this section, accuracy and efficiency of the proposed scheme are evaluated using several examples.

DOI: 10.1002/nag

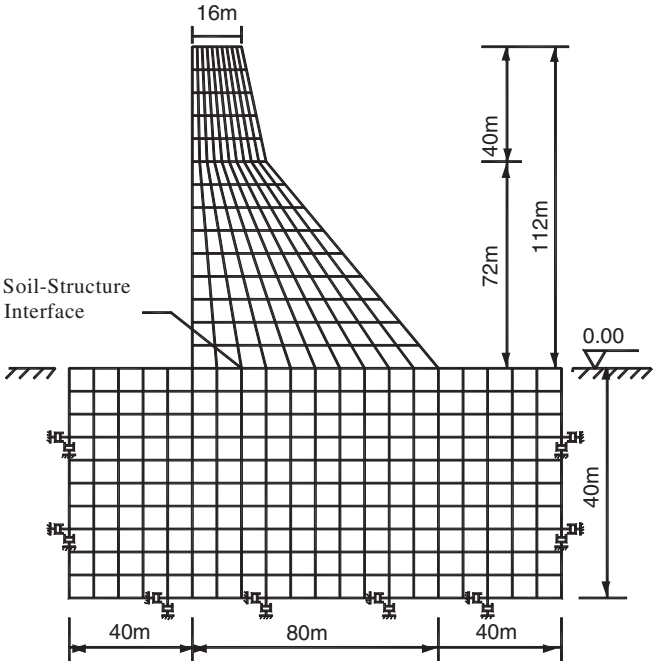

Figure 10. A concrete gravity dam supported by unbounded medium.

4.1. Example 1

The problem used in this example is the third one of the three classical problems investigated by Wolf and Song [8]: a strip foundation with rectangular cross-section embedded in a homogeneous half-plane. The purpose of this example is to verify the feasibility and accuracy of the proposed formulation in computation of the interaction force $\{R^{\infty}(t)\}$.

Referring to Figure 3, the length of the bounded region l is taken to be equal to the characteristic length b, 20 m. The properties of the unbounded medium are assumed as follows: shear modulus $G = 20\,\text{MPa}$, Poisson's ratio $v = 0.25$, and mass density $\rho = 2000\,\text{kg/m}^3$. Viscous dashpots with the coefficients per unit length ρc_{p} (c_{p} is the compressional wave velocity) in the perpendicular direction and ρc_s in the tangential direction on the outer boundary are used as a transmitting boundary.

The transient excitation consists of a harmonic displacement at the centre of the rigid base and in the horizontal direction

$$u_b^{\text{g}}(t) = \begin{cases} \dfrac{u_0}{2}\left(1 - \cos\left(\dfrac{2\pi t}{T}\right)\right), & t \leqslant 2T = 0.8\,\text{s} \\ 0, & t > 2T = 0.8\,\text{s} \end{cases} \tag{30}$$

where the amplitude u_0 is assumed to be 0.2 m and the period of excitation is taken as $T = 8b/c_s = 0.4\,\text{s}$.

DOI: 10.1002/nag

Table II. Material properties of concrete dam and unbounded medium.

	Young's modulus, E (GPa)	Poisson's ratio, v	Density, ρ (kg/m^3)
Concrete dam	20	0.18	2600
Unbounded medium	2.4	0.33	2100

The computed time history of the interaction force is shown in Figure 4(a) for three cases of artificial damping. Here, the dimensionless artificial damping factor, defined as $d = \zeta b/c_s$ [8], is employed. For comparison, the results obtained by only using viscous dashpots on the outer boundary, i.e. without introducing any artificial damping, are also presented. The results, obtained using a sufficiently large region such that the reflected waves do not reach the soil–structure interface in the time of interest, are included as the 'exact' solution.

It is clear from Figure 4(a) that the proposed formulation is feasible and can yield more accurate results than the method only using the viscous boundary. One may note that a satisfactory accuracy can be achieved for the artificial damping factor d of about 1.0–2.0; this is in agreement with the result by Wolf and Song [8].

The importance of extracting the artificial damping in the computation of interaction force is illustrated in Figure 4(b), where the curve denoted as 'bounded damped medium' is obtained by introducing the artificial damping but without extraction. The graph also implies that the analysis by simply using a large damping for the bounded medium cannot lead to a satisfactory solution.

4.2. Example 2

The effect of artificial damping is to attenuate the waves propagating from the soil–structure interface towards the outer boundary and the reflected waves at the boundary. To have a better view of this damping effect, this example investigates the decay with distance of the outgoing wave in terms of its amplitude and energy. The problem analysed is the same with that used in Example 1 but with a larger bounded region (Figure 5): $L = 1100$ m and $b = 50$ m. The properties of the bounded medium are as follows: $G = 5$ GPa, $v = 0.25$, and $\rho = 2000\,\text{kg/m}^3$.

The transient displacement excitation as prescribed by Equation (30) is assumed to act on the soil–structure interface. The duration of the excitation is taken as 1.1 s such that no significant reflected waves are generated on the outer boundary.

The decay of wave amplitude at the ground surface is plotted in Figure 6 against the propagation distance starting from the soil–structure interface (reference location A). Three different values of artificial damping are assumed, i.e. $d = 0.25$, 0.5, and 1.0; the corresponding values of ζ are 5.0, 10.0, and 20.0, respectively. For each value of d, four different periods of excitation, i.e. $T = 0.1$, 0.2, 0.4, and 0.8 s, are investigated.

Figure 6 indicates that the artificial damping can effectively reduce the amplitude of outgoing waves. For $d = 0.25$, the propagation distance required to have a decay rate of 50%, denoted as L_{50}, is about 120 m for all the four cases of excitation period. The distance L_{50} will decrease significantly when a larger damping is used. For example, for $d = 1.0$, L_{50} is approximately 40 m for all the periods considered.

Table I summarizes the propagation distance for a decay rate of 50%, L_{50}, in terms of the wavelength of the propagating wave for all the cases considered. It can be seen that for $d = 0.5$ and $T = 0.1$ s, the amplitude of the propagating wave is reduced by 50% at a propagation distance

DOI: 10.1002/nag

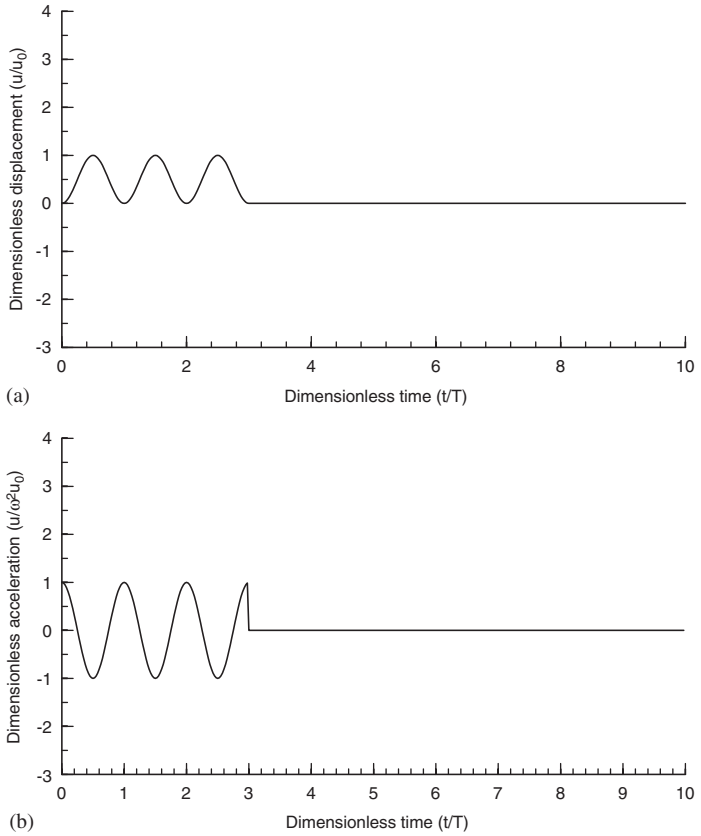

Figure 11. Harmonic excitation used in Example 3: (a) displacement and (b) acceleration.

of 0.8 times the wavelength; while for the same damping factor but a longer period, $T = 0.8$ s, the amplitude is reduced by 50% at a distance of 0.1 times the wavelength.

Since the prescribed excitation is harmonic, it is possible to analytically evaluate the decay of propagating waves. Assuming a shear wave propagating from the interface to the outer boundary, $x = L$, the phase angle is equal to $e^{-i\omega L/c_s}$ if no artificial damping is introduced. Adding the artificial damping will lead to the phase angle being equal to $e^{-i\omega L/c_s} e^{-dL/b}$. Clearly, the additional decay due to the artificial damping is $e^{-dL/b}$. For comparison, the analytical solutions are also included in Figure 6, showing a reasonable agreement with the numerical results.

Another fundamental way to evaluate the effect of artificial damping is to investigate the attenuation of energy during wave propagation. For a specific plane a–a' in Figure 5, the kinetic and potential energy due to wave propagation can be approximately calculated as

$$E_k = \frac{1}{2}\int_a^{a'} \rho \cdot (\dot{u}_x^2 + \dot{u}_y^2)\,dy \tag{31}$$

$$E_p = \frac{1}{2}\int_a^{a'} (\sigma_{xx}\varepsilon_{xx} + \sigma_{yy}\varepsilon_{yy} + \tau_{xy}\gamma_{xy})\,dy \tag{32}$$

DOI: 10.1002/nag

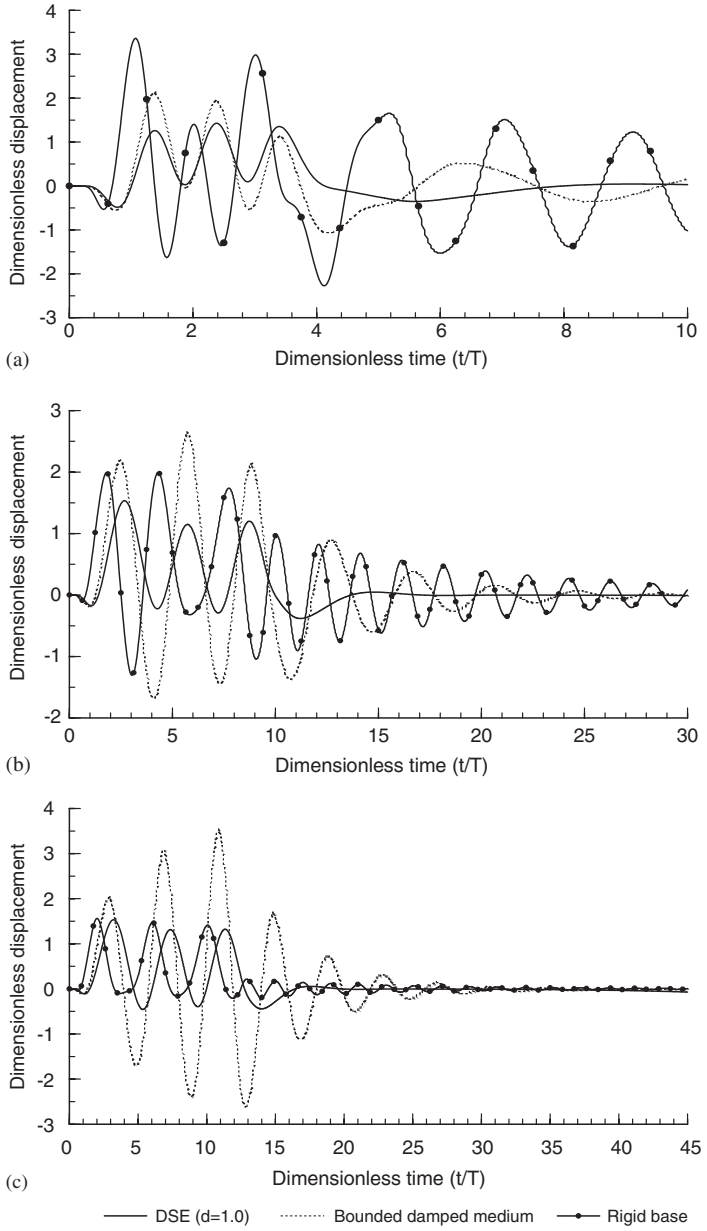

Figure 12. Time history of crest displacement: (a) $T = 0.2$ s; (b) $T = 0.6$ s; and (c) $T = 0.8$ s.

where E_k and E_p denote the kinetic and potential energy, respectively; $\dot{u}_x$ and $\dot{u}_y$ are velocities in horizontal and vertical directions, respectively; σ_{xx}, σ_{yy}, and τ_{xy} are three stress components; ε_{xx}, ε_{yy}, and γ_{xy} are strain components.

DOI: 10.1002/nag

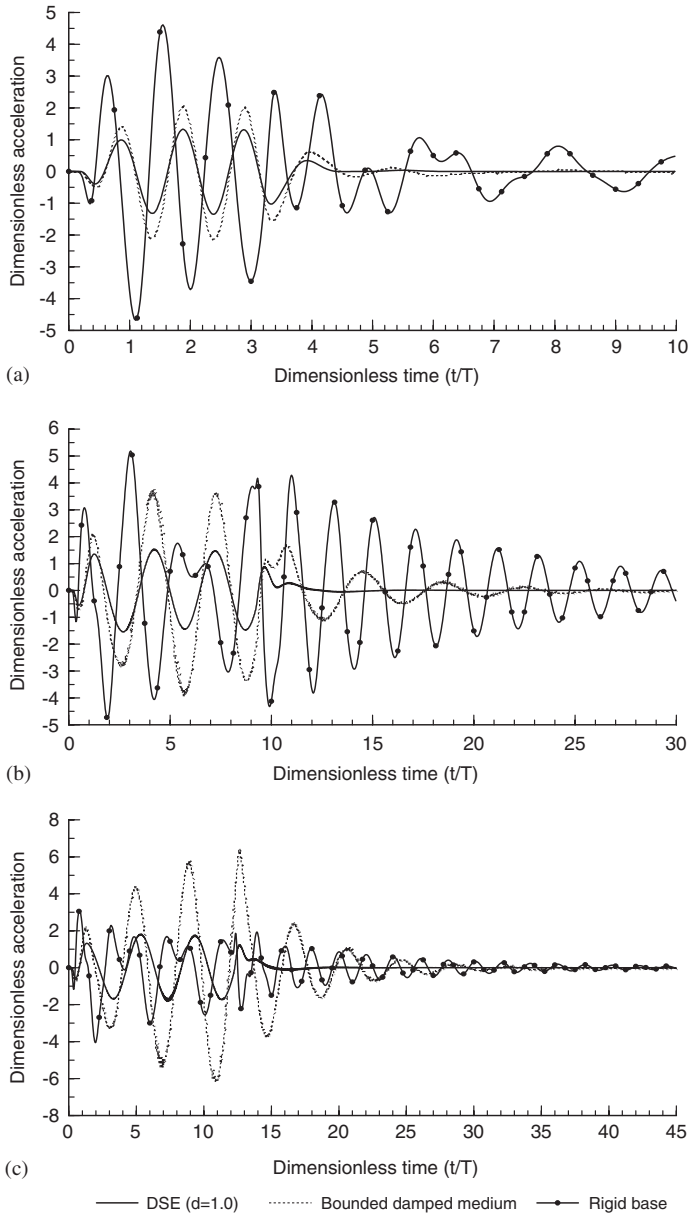

Figure 13. Time history of crest acceleration: (a) $T = 0.2$ s; (b) $T = 0.6$ s; and (c) $T = 0.8$ s.

Using the kinetic and potential energy on the plane A–A' as a reference, Figures 7 and 8 present the decay of the kinetic and potential energy as a function of the propagation distance. In Figure 9 the decay rates for the kinetic and potential energy obtained at $d = 0.5$ and $T = 0.4$ s are compared

DOI: 10.1002/nag

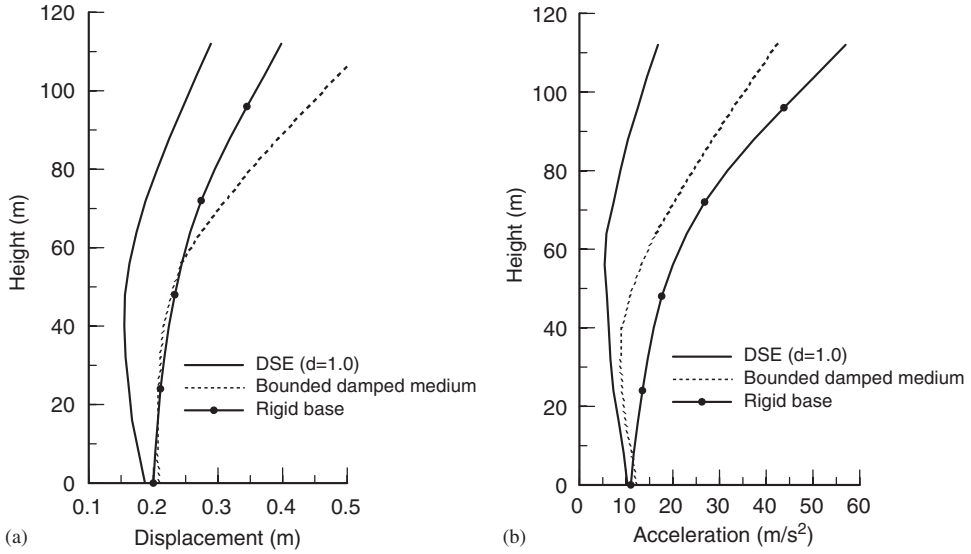

Figure 14. Variation of (a) peak displacement and (b) peak acceleration along dam height ($T = 0.6$ s).

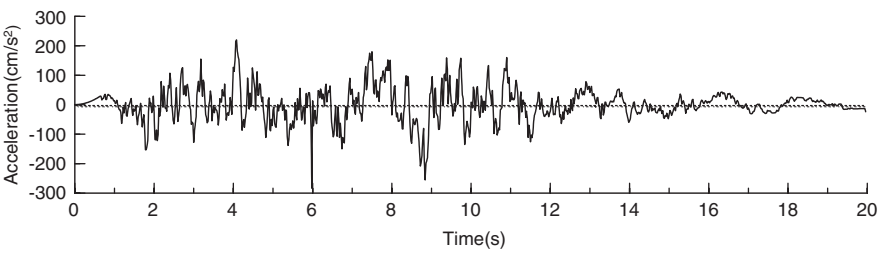

Figure 15. Seismic input acceleration used in Example 3.

with those derived without introducing any artificial damping. These figures clearly illustrate the effect of artificial damping.

4.3. Example 3

The physical model discussed in the first two examples represents an idealized soil–structure interaction problem in which no real structures are involved. In this example, a large-scale soil–structure interaction problem is solved in the time domain, with the purpose of evaluating the feasibility of the proposed scheme in practical applications.

Figure 10 shows a concrete gravity dam supported by unbounded medium. The dam has a height of 112 m, a crest width of 12 m and a base width of 80 m. The material properties of the dam and unbounded medium are given in Table II. In the analysis, a finite bounded region of 40×160 m is selected. The artificial damping factor for the bounded medium is taken to be 1.0. The outer boundary of the finite region is defined as an absorbing boundary.

DOI: 10.1002/nag

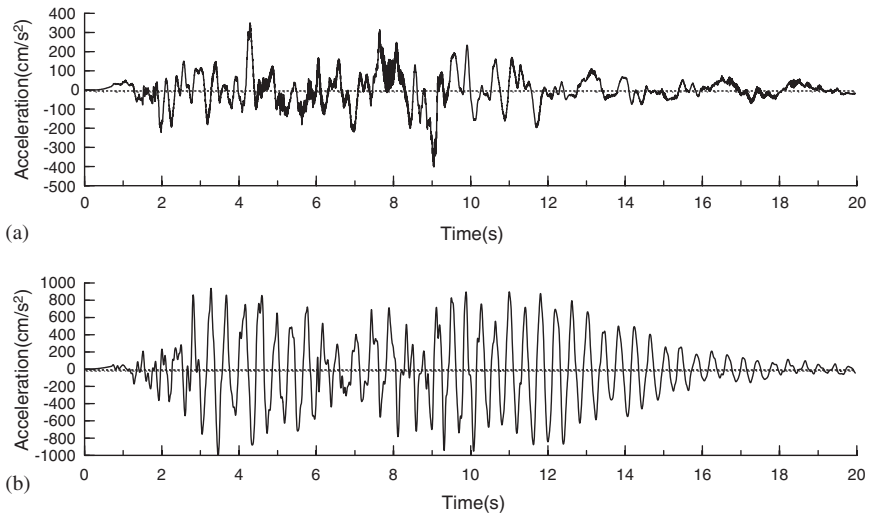

Figure 16. Acceleration response at dam crest computed using (a) DSE method and (b) rigid-base model.

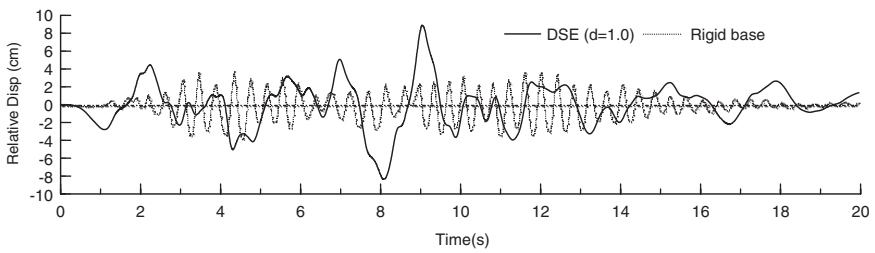

Figure 17. Time history of relative displacement at dam crest.

First, consider the harmonic input motions shown in Figure 11 in the dimensionless form, where the amplitude of displacement excitation, u_0, is assumed as 0.2 m. Three different excitation periods, i.e. $T = 0.2$, 0.6, and 0.8 s, are investigated.

Figure 12 presents the computed displacement response at dam crest for the three cases of excitation period, and Figure 13 shows the corresponding acceleration response at dam crest. Note that both the crest displacement and crest acceleration are normalized by the amplitudes of input motions, and thus the response can be regarded as the amplification factor. To view the effectiveness of the time-domain DSE method, the results obtained using the same amount of artificial damping but without extraction (denoted as bounded damped region) and the results obtained by assuming a rigid base (i.e. ignoring soil–structure interaction) are also included in Figures 12 and 13. The comparisons indicate that appropriate modelling of the unbounded medium is critical to the response of the dam.

Figure 14 shows the amplitude distribution of the displacement and acceleration along the height of the dam. One may note that, compared with the DSE method, the other two methods of modelling the unbounded medium give higher estimates of both the displacement and acceleration.

DOI: 10.1002/nag

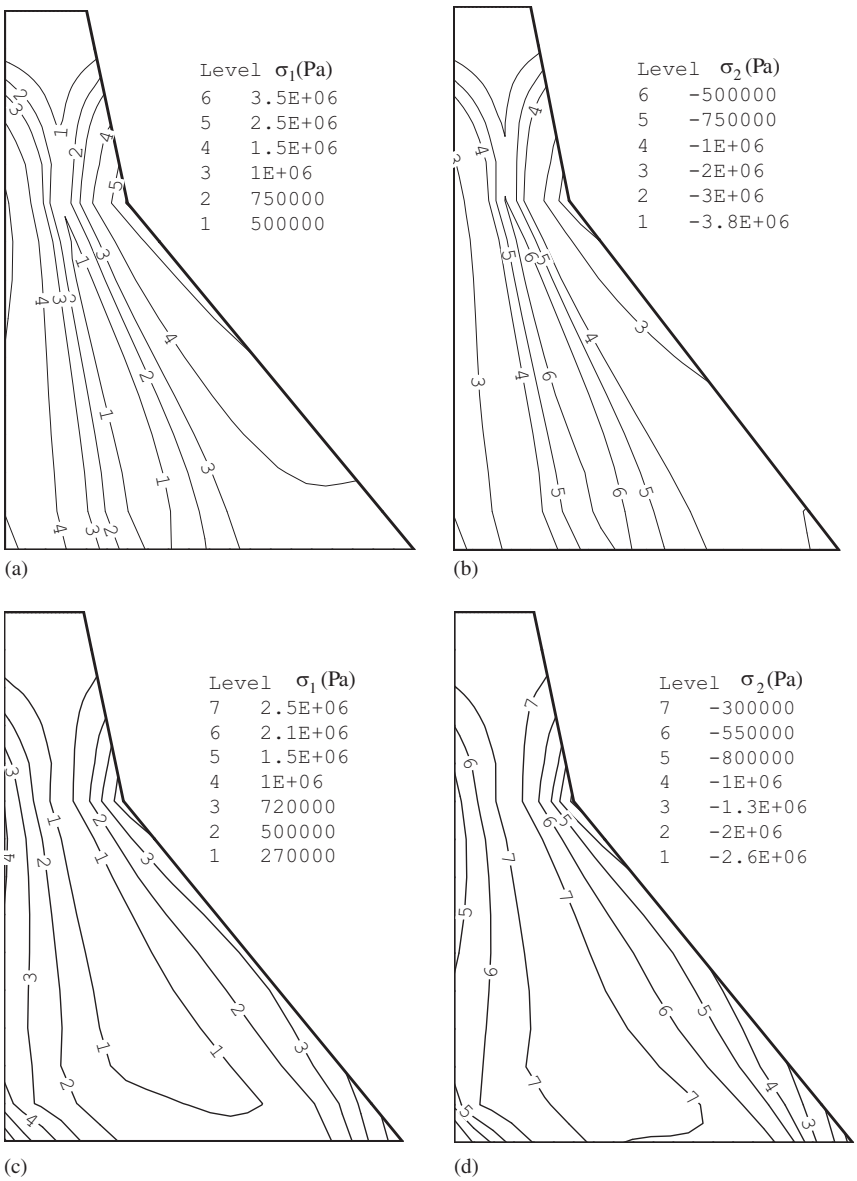

Figure 18. Contours of peak principal stresses within dam: (a) tensile and (b) compressive stresses computed using rigid-base model; (c) tensile and (d) compressive stresses computed using DSE method.

Now, consider a random seismic excitation shown in Figure 15. The response of the crest acceleration to this excitation, computed using the time-domain DSE scheme, is shown in Figure 16 along with the response computed using the rigid-base model. Figure 17 compares the time histories of the relative displacements at dam crest obtained for the two models of the unbounded medium.

DOI: 10.1002/nag

It is seen that the rigid-base model yields an unreasonably great acceleration response but a much smaller estimate of the relative displacement.

Figure 18 illustrates the contours of the principal compressive and tensile stresses within the concrete dam. Compared with the DSE method, the rigid-base model is found to overestimate both the principal compressive and tensile stresses in the dam. The maximum compressive and tensile stresses in the dam calculated using the rigid-base model are 3.65 and 3.87 MPa, respectively, and they reduce to 2.62 and 2.84 MPa, respectively, when the DSE method is used. Moreover, it is noted that the DSE method predicts a stress concentration occurring at the toe and heel of the dam but this feature does not appear in the predictions using the rigid-base model.

5. CONCLUSIONS

This paper presents a subregional stepwise damping solvent extraction formulation for time-domain analysis of soil–structure interaction problems. The formulation avoids the use of convolution integrals and eliminates the time variable in the computation of the interface force. This renders it suitable for the analysis of large-scale dynamic problems. A detailed evaluation of the performance of the formulation has been carried out for a strip foundation embedded in a half-space and subjected to a harmonic excitation. The analysis shows that the formulation is effective and the degree of accuracy depends on the value of the dimensionless damping factor d (associated with the artificial nodal damping coefficient ζ). Generally, $d = 1.0$ gives a highly accurate solution.

The proposed method has been applied to a large-scale dynamic soil–structure interaction problem that represents a high concrete gravity dam subjected to seismic load. The comparison of the various responses of the dam with those obtained using other models for the unbounded medium indicates that the method is feasible and efficient for solving practical dynamic interaction problems.

ACKNOWLEDGEMENTS

The support provided by the Natural Science Foundation of China (90510018) and the Research Grants Council of Hong Kong (HKU7191/05E) is gratefully acknowledged.

REFERENCES

1. Wolf JP. *Soil–structure Interaction Analysis in Time Domain*. Prentice-Hall: Englewood Cliffs, NJ, 1988.
2. Dominguez J. *Boundary Elements in Dynamics*. Computational Mechanics Publishing: Southampton, 1993.
3. Manolis GD, Beskos DE. *Boundary Element Methods in Elastodynamics*. Unwin Hyman: London, 1988.
4. Clayton R, Engquist B. Absorbing boundary conditions for acoustic and elastic wave equations. *Bulletin of the Seismological Society of America* 1977; **67**:1529–1540.
5. Liao ZP, Wong HL. A transmitting boundary for the numerical simulation of elastic wave propagation. *Soil Dynamics and Earthquake Engineering* 1984; **3**:174–183.
6. Lysmer J, Kuhlemeyer RL. Finite dynamic model for infinite media. *Journal of Engineering Mechanics Division* (ASCE) 1969; **95**(EM4):859–877.
7. Smith WD. A nonreflecting plane boundary for wave propagation problems. *Journal of Computational Physics* 1974; **15**:492–503.
8. Wolf JP, Song Ch. *Finite-element Modeling of Unbounded Media*. Wiley: New York, 1996.
9. Basu U, Chopra AK. Numerical evaluation of the damping-solvent extraction method in the frequency domain. *Earthquake Engineering and Structural Dynamics* 2002; **31**:1231–1250.

DOI: 10.1002/nag

10. Zhang X, Wegner JL, Haddow JB. Three-dimensional dynamic soil–structure interaction analysis in the time domain. *Earthquake Engineering and Structural Dynamics* 1999; **28**:1501–1524.
11. Hughes TJR, Liu WK. Implicit–explicit finite elements in transient analysis: stability theory. *Journal of Applied Mechanics* (ASME) 1978; **45**:371–374.
12. Hughes TJR, Liu WK. Implicit–explicit finite elements in transient analysis: implementation and numerical examples. *Journal of Applied Mechanics* (ASME) 1978; **45**:375–378.
13. Berg GV, Housner GW. Integrated velocity and displacement of strong earthquake ground motion. *Bulletin of the Seismological Society of America* 1961; **51**:175–189.
14. Boore DM. Effect of baseline corrections on displacements and response spectra for several recordings of the 1999 Chi-Chi, Taiwan, Earthquake. *Bulletin of the Seismological Society of America* 2001; **91**:1199–1211.
15. Trifunac MD. Zero baseline correction of strong-motion accelerograms. *Bulletin of the Seismological Society of America* 1971; **61**:1201–1211.
16. Yang J, Li JB, Lin G. A simple approach to integration of acceleration data for dynamic soil–structure interaction analysis. *Soil Dynamics and Earthquake Engineering* 2006; **26**:725–734.

DOI: 10.1002/nag